International Journal of Pharmaceutics 510 (2016) 1–8

Contents lists available at ScienceDirect

International Journal of Pharmaceutics

journal homepage: www.elsevier.com/locate/ijpharm

Application of X-ray microtomography for the characterisation of hollow polymer-stabilised spray dried amorphous dispersion particles

John F. Gamble[a,*], Masako Terada[b], Christian Holzner[b], Leah Lavery[b], Sarah J. Nicholson[a], Peter Timmins[a], Mike Tobyn[a]

[a] Bristol-Myers Squibb, Reeds Lane, Moreton, Wirral, CH46 1QW, UK
[b] Carl Zeiss X-ray Microscopy, 4385 Hopyard Rd., Suite 100, Pleasanton, CA 94588, USA

ARTICLE INFO

Article history:
Received 18 February 2016
Received in revised form 24 May 2016
Accepted 26 May 2016
Available online 1 June 2016

Keywords:
Spray drying
Spray dried dispersion
Powder properties
Density
Imaging
Pharmaceuticals

ABSTRACT

The aim of this study was to investigate the capability of X-ray microtomography to obtain information relating to powder characteristics such as wall thickness and solid volume fraction for hollow, polymer-stabilised spray dried dispersion (SDD) particles. SDDs of varying particle properties, with respect to shell wall thickness and degree of particle collapse, were utilised to assess the capability of the approach.

The results demonstrate that the approach can provide insight into the morphological characteristics of these hollow particles, and thereby a means to understand/predict the processability and performance characteristics of the bulk material. Quantitative assessments of particle wall thickness, particle/void volume and thereby solid volume fraction were also demonstrated to be achievable. The analysis was also shown to be able to qualitatively assess the impact of the drying rate on the morphological nature of the particle surfaces, thus providing further insight into the final particle shape.

The approach demonstrated a practical means to access potentially important particle characteristics for SDD materials which, in addition to the standard bulk powder measurements such as particle size and bulk density, may enable a better understanding of such materials, and their impact on downstream processability and dosage form performance.

1. Introduction

The use of dissolution enhancing approaches during pharmaceutical formulation development activities is now increasing in utility and a range of mature technologies are available. This is particularly so when more traditional approaches such as size reduction (Rabinow, 2004) and the use of salts (Berge et al., 1977) or pro-drugs (Rautio et al., 2008) are unable to give sufficient increases in solubility/bioavailability in order to make the crystalline drug substance viable for use in a standard solid dosage form. As the number of compounds with low solubility (BCS class II and IV) increases, the use of amorphous solid dispersions (Bhugra and Pikal, 2008; Chiou and Riegelman, 1971; Ford, 1986; Hancock and Parks, 2000; Leane et al., 2013; Leuner and Dressman, 2000; Serajuddln, 1999) is correspondingly becoming more common. Spray drying and hot melt extrusion, to produce stabilised amorphous systems, is becoming a standard means to achieve the necessary dissolution.

Spray drying involves the rapid drying of an atomised feed solution consisting of organic solvent(s) containing an active pharmaceutical ingredient (API) plus any additional components such as polymers used to provide a stabilised amorphous systems (Paudel et al., 2013; Tobyn et al., 2009; Wegiel et al., 2013; Yoshioka et al., 1995). In such stabilised amorphous systems the role of the polymer can be to increase the glass transition temperature of the intermediate material and inhibit mobility of the constituents (kinetic stabilization) (Hancock et al., 1995), provide a matrix in which the amorphous active is soluble (thermodynamic stabilization) (Baird and Taylor, 2012; Van den Mooter et al., 2000), improve wetting during dissolution, and following dissolution to form a super-saturated solution to inhibit crystallization from solution (Alonzo et al., 2010; Graeser et al., 2009; Vandecruys et al., 2007). The polymer can also play a role in the chemical stabilization of the drug within the spray dried dispersion (SDD) matrix (Patterson et al., 2015).

Particle formation during spray drying is achieved by atomizing the feed solution to form droplets, the size of which is dependent

* Corresponding author at: Bristol-Myers Squibb, Reeds Lane, Moreton, Wirral, UK.
E-mail address: john.gamble@bms.com (J.F. Gamble).

http://dx.doi.org/10.1016/j.ijpharm.2016.05.051
0378-5173/

on the nozzle design, spray pressure, and feed solution viscosity (Elversson et al., 2003). As the droplets begin to dry a film is formed around the outer edges of the droplet following which the exterior dimension of the particle remains relatively fixed. As drying progresses, the remaining solvent is driven off thereby creating a void space within the SDD particle. Dependent on the rate of drying, these voids can be expressed in multiple ways, from a single central void space at one extreme, to a porous honeycomb type structure at the other (Maher et al., 2015; Vehring, 2008; Vehring et al., 2007). The thickness of the particle wall will define the amount of solid present within a particle rather than the volume of the particle, and may also control the rate of drying in subsequent secondary drying steps (Hsieh et al., 2015). Hollow SDD particles may additionally undergo partial collapse forming raisin-like particles with the final morphology being dependent on the drying conditions used (Vicente et al., 2013).

In previous work, the use of mercury intrusion (Yates et al., 2015), imaging technologies such as cryogenic scanning electron microscopy (SEM) and image based particle characterization (Gamble et al., 2014) have been applied to understand the impact of spray drying parameters on particle attributes such as wall thickness and solid volume fraction. In the latter work it was demonstrated that the use of tests such as bulk density did not adequately describe the particle characteristics as the measurement, in addition to particle size and the packing of the particles, was also affected by variations in the volume of the internal void space within the particles. Whilst the measurements made were shown to be informative, the methodology applied was inherently prone to bias, due to the low number of particles analysed, and very labour intensive, making the approach practically infeasible for routine analysis.

The above approach also utilised a number of assumptions, a key assumption being the particles (and the void spaces) were spherical in nature, which excludes application of the approach to SDD particles which have undergone some degree of collapse during drying, a feature commonly observed for many polymer stabilised SDD materials.

In an attempt to overcome these limitations, X-ray microtomography (XRM) was assessed as an alternative approach to elucidate the morphological nature of SDD particles. XRM has been previous demonstrated to be able to measure the internal structure of SDD materials (Wong et al., 2014a) due to the sensitivity of the technique to density differences within samples.

The aim of this work was to investigate the feasibility of XRM to characterize SDD materials. For the purposes of this feasibility study, samples of SDD materials with as wide a range of morphological characteristics were analysed in order to fully assess the ability of the XRM to deal with varying wall thicknesses and extent of particle wall collapse. SDD material of varying wall thickness which had previously been characterised and reported (Gamble et al., 2014) were analysed to assess the feasibility of XRM. In addition, samples of SDD showing varying levels of wall collapse were also analysed to assess the ability of the approach to characterize the 3-dimensional internal pore volume characteristics and wall thicknesses of such particles. As a consequence of the sample selection process, an in-depth investigation of the inter-relationship between spray drying conditions and particle characteristics was out of scope for this initial study.

2. Materials

The materials used during this study were:

a) A spray dried amorphous dispersion consisting of 90.9% BMS-817399 (Bristol-Myers Squibb, USA) (Santella et al., 2014), and 9.1% PVP K-30 (Ashland Inc., Covington, KY, USA). The drug substance has a melting point of 210 °C and a glass transition temperature of 123 °C. The three batches used, batches B, D and E, were obtained using the methods previously reported (Gamble et al., 2014) and the same batch references are used to provide clarity across both pieces of work.
b) Batch F was a spray dried amorphous dispersion consisting of 40% BMS-708163 (Bristol-Myers Squibb, USA) (Gillman et al., 2010), and 60% HPMC-AS (ShinEtsu Chemical Co. Ltd., Japan). The drug substance has a melting point of 160 °C and a glass transition temperature of 45 °C. The batch was subsequently tray dried to remove residual solvent.
c) Batch G was a spray dried amorphous dispersion consisting of 100% HPMC-AS (ShinEtsu Chemical Co. Ltd., Japan). The batch was subsequently tray dried to remove residual solvent.

3. Methods

3.1. Spray drying process

The spray dried dispersions used in this study were all manufactured on a GEA Niro PSD-1 or PSD-2 spray dryer (GEA Niro, Columbia, USA). The API and polymer were first dissolved in the selected solvent system before being sprayed; the spray drying conditions for all lots studied are detailed in Table 1. The relative saturation at the outlet ($\%RS_{out}$) for the three BMS-817399 SDD lots was calculated based upon the approach reported by Dobry et al. (2009) as shown in Eq. (1):

$$\%\mathrm{RS}_{\mathrm{out}} = 100.\left(\frac{\mathrm{P}_{\mathrm{chamber}}}{\mathrm{P}^{*}_{\mathrm{T}_{\mathrm{out}}}}\right).\frac{\mathrm{M}_{\mathrm{soln}}\left(1-\chi_{\mathrm{solids}}\right)/\mathrm{MW}_{\mathrm{solvent}}}{\left(\frac{\mathrm{M}_{\mathrm{soln}}\left(1-\chi_{\mathrm{solids}}\right)}{\mathrm{MW}_{\mathrm{solvent}}}+\frac{\mathrm{M}_{\mathrm{gas}}}{\mathrm{MW}_{\mathrm{gas}}}\right)} \quad (1)$$

where M_{soln} is the solution feed rate, M_{gas} is the drying-gas flow rate, T_{out} is the drying-gas outlet temperature, χ_{solids} is the mass fraction solids in solution, $MW_{solvent}$ and MW_{gas} are the molecular weights for the respective species, P_{chamber} is the absolute pressure

Table 1
Spray drying conditions for investigatory batches.

Material	Batch reference	Polymer	API load (%)	Spray solvent	Spray dryer	Solids concentration in solution (%w/w)	Solution temperature (°C)	Atomizing pressure (psi)	Inlet temperature (°C)	Outlet temperature (°C)	Solution feed rate (g/min)
BMS-817399	Batch B	PVP K-30	90.9	Methanol	PSD-1	35	Ambient	150	113	40	140
	Batch D					35		150	143	60	
	Batch E					25		125	124	40	
BMS-708163	Batch F	HPMC-AS	40	Acetone	PSD-2	16	Ambient	400	98	31	1167
Placebo SDD	Batch G	HPMC-AS	0	90:10 Methanol: water	PSD-1	7.5	121	248	151	88	145

in the spray-dryer chamber, and P^*_{Tout} is the equilibrium vapor pressure of the spray solvent evaluated at T_{out}.

3.2. X-ray microtomography

The samples were prepared by pouring an aliquot of each SDD material into a Kapton tube (Carl Zeiss, Pleasanton, CA, USA) which was then sealed using tissue paper and epoxy. The Kapton tube was attached to aluminium rod adaptor and then mounted on a ZEISS sample holder (Carl Zeiss, Pleasanton, CA, USA). No compression was applied to the samples in order to prevent any artificial modification of the particle morphology.

The samples were analysed using an Xradia 510 Versa 3D X-ray Microscope (Carl Zeiss Microscopy, Pleasanton, CA, USA). The instrument has a polychromatic transmission source with a tungsten target that allows up to 160 kV and projects the sample in a cone beam geometry onto a detector. The sample was imaged at 40 kV and a power of 3 W with no applied beam spectrum filter. The sample-detector and source-sample distances were set at 13 mm and 8 mm, respectively resulting in an isotropic voxel size of 0.5 μm. Instead of a single flat panel detector, the instrument incorporates a unique detector design with a set of multiple objective lens coupled to a CCD (2048 × 2048 pixels with 13.5 μm pixel size), which results in selectable field of view pairings. In this study, the 20X objective lens was used with a total field of view of 1.3 × 1.3 mm resulting a spatial resolution of 0.9 μm. For each sample, 3201 projections over 360° were obtained, with an exposure time of 15 s per projection, resulting in a total scanning time of 15 h. In order to ease with subsequent segmentation and analysis of the reconstructed volumetric data, the individual projections were filtered with a Paganin-type single distance phase retrieval method as described in (Mayo et al., 2002). The data was then reconstructed using a standard filtered back projection algorithm for cone beam tomography including a 3D Gaußian filter of 0.5 voxel FWHM. Data visualization and analysis was completed in ORS Visual SI Advanced software (Object Research Systems, Montreal, Canada).

3.3. Scanning electron microscopy (SEM)

Samples were sputter coated with gold using a JFC-1300 auto fine coater (Jeol Inc., MA, USA); the samples were then imaged using a Neoscope JCM-500 (Jeol Inc., MA, USA) using an accelerating voltage of 10–30 kV.

3.4. Bulk and tapped bulk density

To obtain the bulk density, approximately 60 ml of each sample was added to a 100 ml graduated cylinder of known mass with minimal agitation and the mass and exact volume recorded. The tapped powder volume was then obtained after 1000 taps using a Vankel bulk and tap density apparatus (Vankel, Cary, USA).

3.5. True density

The true density of the materials was determined using helium pycnometry (AccuPyc II 1340, Micromeritics Instrument Co., Norcross, GA, USA). Samples were dried at 50 °C for at least 12 h prior to analysis. Calibration of the AccuPyc was performed using two standard stainless steel balls of known mass and volume.

4. Results and discussion

4.1. Comparison of XRM and Cryogenic SEM data

To assess the ability of the technique to measure the three dimensional void space of SDD particles, three samples of BMS-817399:PVP K-30 (90.9% API:9.1% polymer) SDD which had previously been analysed using a cryogenic SEM approach (Gamble et al., 2014) were assessed. The morphological nature of these SDD samples was that of highly spherical, non-collapsed particles with some degree of fragmentation.

Previous work, using two dimensional images to calculate three dimensional solid volume fractions, had demonstrated that all three samples had varying wall thicknesses and solid volume fractions (SVF), thus the comparison against XRM findings would enable some degree of validation of the new approach, whilst also testing the limitations of the original measurement. For the purposes of the SVF measurement, data for 20 randomly selected particles from each lot was generated, with the void space analysis conducted using ORS Visual SI Advanced software (Object Research Systems, Montreal, Canada).

An initial challenge with the new approach was that differentiation between the inter-particular and intra-particular voids could not be made automatically due to the density of both being equivalent and as a consequence, extraction of the void data was labour intensive. The reason for this issue was related to the simplified sample preparation methodology utilised for the purposes of this trial. The technology measures density differences, and hence is able to detect SDD shell walls. However, as the samples were loosely packed into the sample holder, the density of the intra and inter-particulate void spaces was equal, thus making discrimination of the SDD particle shells non-automatable.

Despite this challenge, the image data generated was able to extract information relating to the wall thickness and the actual 3-dimensional solid volume fraction of particles within each sample thus enabling the data to be compared to that of the original cryogenic SEM analysis (Fig. 1).

The XRM results were observed to provide generally equivalent solid volume fractions measurements to those obtained by the cryogenic SEM approach thus confirming the previously measured differences in solid volume fraction for the three batches. This data confirmed that for the purposes of these particles, generally non-collapsed SDD particles, the assumptions made for the cryogenic SEM analysis (i.e. material consisting primarily of spherical, non-collapsed particles) did not negatively affect the accuracy of the method.

In addition to SVF measurements, the XRM data was able to provide qualitative information about the morphological nature of the particles. Whilst the images confirm that the particles are indeed highly spherical in nature with a well-defined spherical internal void space, some differences in the smoothness of the external surface of the particles could be observed, with particles from batches manufactured with higher outlet temperatures/lower relative outlet saturation levels observed to be more smooth

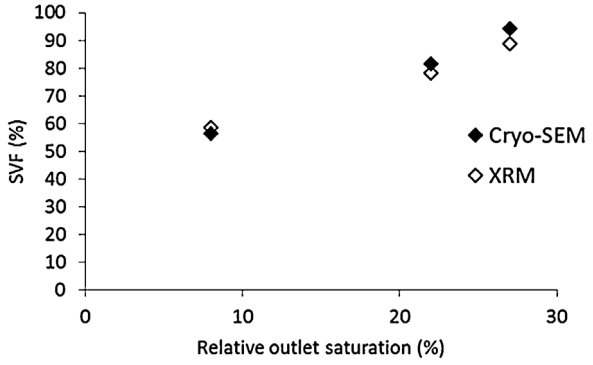

Fig. 1. Plot of relative outlet saturation versus particle solid volume fraction measured by XRM (◇) and calculated from cryogenic SEM images (◆).

and less pitted, a probable consequence of the relative drying rates of the particles (Fig. 2).

By taking multiple measurements of the wall thickness of particles in each lot, false colour images showing the distribution of wall thicknesses across the particles within lots (Fig. 3) and representations of the particles with the void spaces could also be generated (Fig. 4). For these two samples, if the distribution of wall thicknesses is plotted in terms of the arithmetic (numerical) frequency (Fig. 5), it could be demonstrated that batch B consists of particles with a wider range of wall thicknesses than batch D, which is observed to consist, relatively, of thinner walled particles.

This type of information may provide increased understanding into the processability and performance such materials. In terms of processability, the particle density will impact the powder flow characteristics as well as the propensity for adhesion; in the latter case, the impact of static charging may affect much larger SDD particles than in solid particles due to the low relative mass per unit volume of the particles (Murtomaa et al., 2004; Wong et al., 2014b). With respect to performance, dissolution of such particles may be slower for thicker walled particles if the mechanism of drug release is erosion based whilst compressibility and compactibility may also be affected by the wall thickness/solid volume fraction.

These results clearly demonstrate that XRM could indeed be applied to the characterisation of SDD particles, but the applicability of the approach to more typical, partially collapsed particles was the ultimate aim of the work.

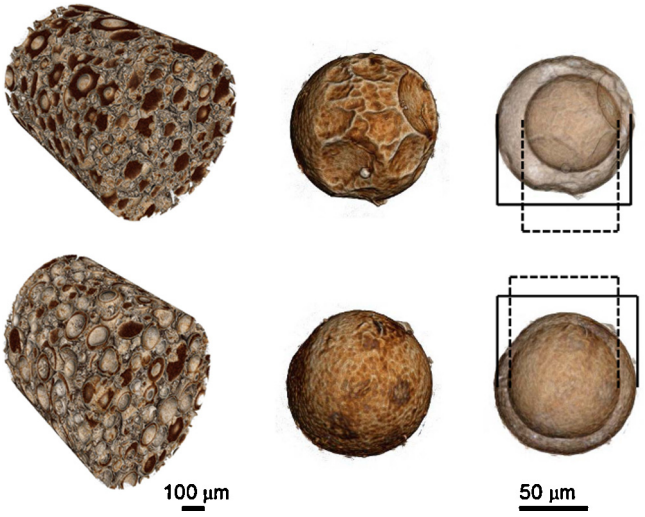

Fig. 2. Reconstructed images of SDD powder bed showing surface/topology and the intra-particulate void space/wall thickness for an example particle from each of two batches of BMS-817399 (Top = Batch B; Bottom = Batch D).

4.2. Application to SDD particles with collapsed walls

Although SDD particles are generally described as spherical particles, most pharmaceutical stabilised amorphous SDDs are, to lesser and greater extents, partially collapsed, leading to descriptions such as 'raisin-like' (example shown in Fig. 6). For such particles, the assumption of sphericity for volume/void calculations is not valid and therefore measurements using approaches such as the cryogenic SEM method will inevitably lead to inaccurate estimations and may also be prone to artefacts related to the vacuum process used to generate the images. Consequently, the ability of any approach to obtain equivalent information for less ideal, and thereby more realistic SDD particles is highly desirable.

The use of X-ray microtomography was proposed as a solution to this issue and so samples of SDDs with varying degrees of particle wall collapse were analysed. In addition to one of the previous discussed non-collapsed samples (Batch E), two additional SDD materials were analysed; a partially collapsed, generally spherical SDD (BMS-708163, Batch F) and a highly collapsed placebo SDD (HPMC-AS, Batch G) prepared by spraying the solution at temperatures above the solvent boiling point (Fig. 6).

Spray drying using solution temperatures above the boiling point of the solvent can be utilised for manufacturing SDDs from actives with relatively low solubility in the spray solvent. In such processes, a suspension of the active in a solvent solution of the excipients is heated in-line to a high enough temperature that the active fully dissolves in the solution prior to atomization. As a consequence of the high temperature the solvent undergoes flash atomisation rather than pressure induced atomisation. This change of atomisation tends to result in SDD particles with a highly collapsed morphology.

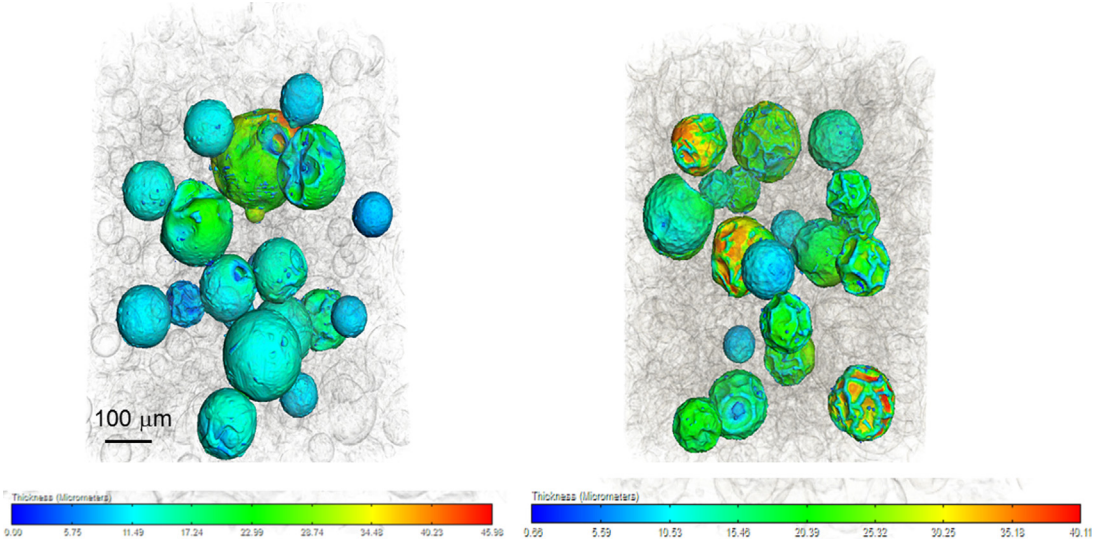

Fig. 3. Image of example SDD particles extracted from the powder bed for two batches of BMS-817399 (Left image = Batch B; Right image = Batch D). Particle surface colour corresponds to variations in the particle shell wall thickness.

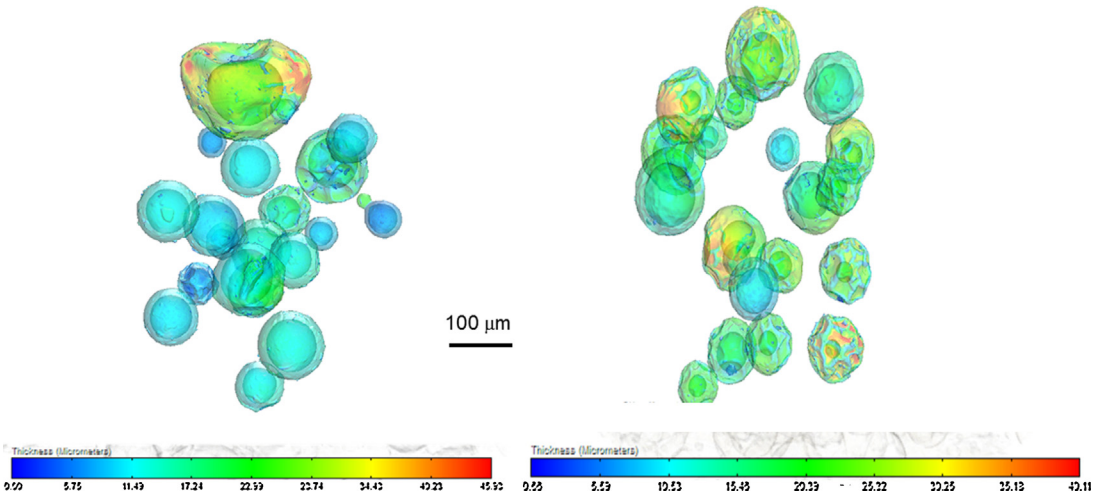

Fig. 4. Image of example SDD particles extracted from the powder bed for two batches of BMS-817399 (Left image = Batch B; Right image = Batch D) showing intra-particulate void spaces.

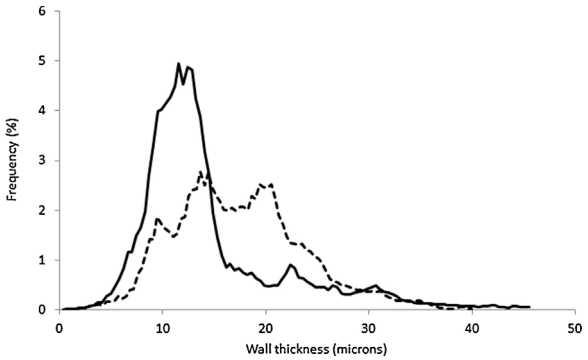

Fig. 5. Frequency plot of particle shell wall thickness measurements for two batches of BMS-817399 (Dashed line = Batch B; Solid line = Batch D).

The samples were analysed using the same approach as the previous samples; example X-ray microtomography planes for all three materials, along with a 3-dimensional reconstruction of a typical particle from each of the lots is shown in Fig. 7.

In order to improve the ability to separate the individual particles/elements of the measured particles a semi-automated phase contrast filtering (Mayo et al., 2002) approach was utilised. This approach was demonstrated to provide a significant improvement in the ability to segment the particles, thereby enabling larger sample populations (~100 particles) to be extracted for the non-collapsed and partially collapsed datasets. The approach was not able to improve the separation for the very highly collapsed particles (Batch G), however, data for a small population of particles from this material could still be extracted using manual filtering approaches. Further work to establish how best to improve the filtering to further increase particle numbers and better enable automated extraction will continue with particular focus on the highly collapsed particles. For future work, the use of an inert support medium to better differentiate intra and inter-particulate voids could be introduced in order to provide three distinct densities thus aiding the filtering capabilities.

As previously discussed, the BMS-817399 SDD (Batch E) particles were observed to be primarily spherical but with the presence of fragmented SDD particles due to the previously reported friability of this material (Gamble et al., 2014). As expected from the work described in the previous section, these particles were observed to have thick walls, with wall thicknesses typically in the range of 10–30 μm and relatively small intra-particular void spaces, hence the material was determined to have a percentage SVF of approximately 89%.

The BMS-708163 SDD particles (Batch F) were observed to be a mixture of spherical and ovoid shaped particles with somewhat irregular wall thicknesses suggesting partial collapse/droplet fusion. The walls were relatively thin, typically in the 2–10 μm range, with most particles observed to have large intra-particular void spaces. Consequently, the SVF of this material was observed to be the lowest of the SDD lots analysed with a percentage SVF of approximately 38%.

The placebo SDD (Batch G), being highly collapsed in nature, was included in the study to test the limitations of the XRM approach. The wall thicknesses of these particles were found to be

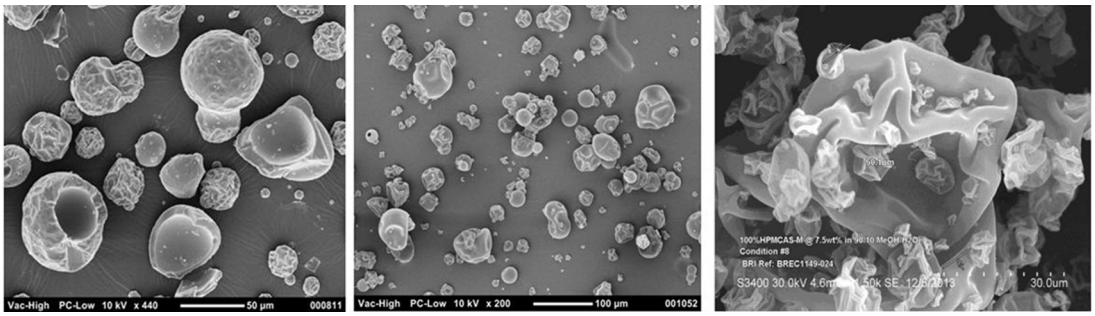

Fig. 6. SEM images of SDDs tested (left to right, BMS-817399 batch E, BMS-708163 batch F and HPMC-AS Batch G).

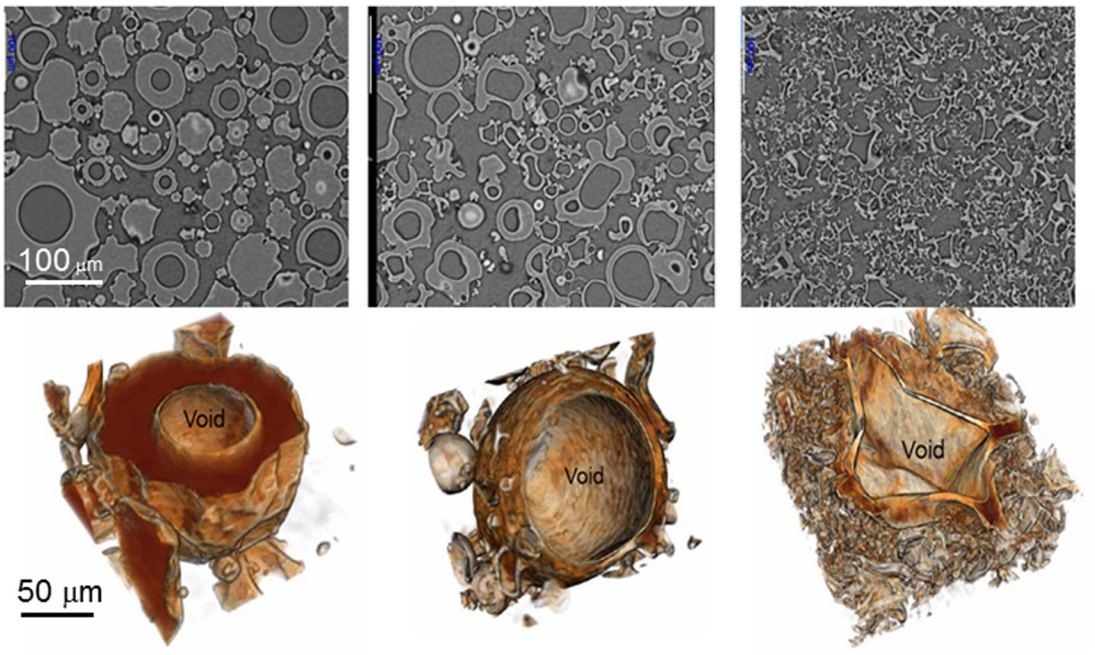

Fig. 7. Example single plane XRM image and example of reconstructed 3-dimensional particle with void space for each of the three materials analysed (left to right, BMS-817399 batch E, BMS-708163 batch F and HPMC-AS batch G).

much lower than the other two SDD materials, typically in the range of 1–2 µm.

Despite the high degree of the particle wall collapse, the particles were observed to be complete, intact particles containing large, clearly defined intra-particular void spaces. Although these particles did have the thinnest walls of all SDDs tested, the percentage SVF of these particles was found to be intermediate of the other two materials with a value of approximately 62%.

As the wall thicknesses of these particles are small, the measured SVF is more directly related to the extent of wall collapse, thus leading to reductions in the particle volume and thereby an increase in the solid mass per unit volume of the overall particle. Whilst this material was found to have an intermediate solid volume fraction, the bulk density of the material was the lowest of the three SDDs (Fig. 8).

The lack of a trend in the relationship between bulk density and solid volume fraction for the three materials is expected. The SVF, being a ratio of volumes, is affected solely by the wall thickness (the solid volume) and the degree of wall collapse (the particle volume), whereas bulk density is, in addition to the above factors, also affected by particle size and particle packing within a powder bed.

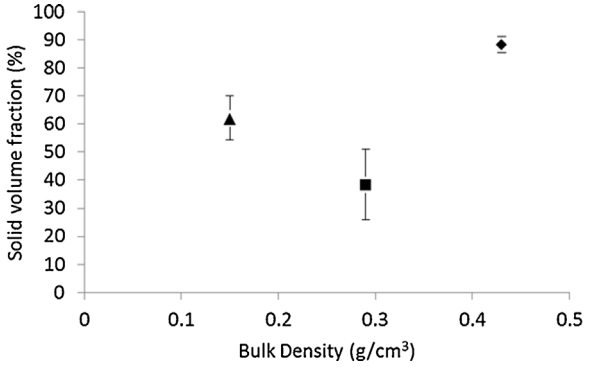

Fig. 8. Plot of the measured solid volume fraction (range and mean) versus bulk density for the three analysed materials (▲ = BMS-817399 batch E; ■ = BMS-708163 batch F; ◆ = HPMC-AS batch G).

If the bulk density is explained in terms of porosity (ϕ), for solid particles, the powder bed porosity (ϕ_{bulk}) of a powder bed is simply the inter-particulate void space present per unit mass of particles. Therefore, if the volume of solid (through measurement of the mass and true density) and the volume of the powder bed is known, the inter-particulate void space for the bed, i.e. the powder bed porosity (ϕ_{ip}) can be extracted.

For SDD materials a similar relationship can be proposed where the bed porosity is the sum of the inter-particulate void space and the intra-particulate void space (ϕ_p). The mean particle porosity for the materials can be extracted from the measured XRM results by means of the apparent true density of the particles. Using this approach, one can therefore determine the fraction of volume present in the intra-particulate void spaces (related to particle morphology) and the inter-particulate void space (related to packing within the powder bed) by means of Eq. (1).

$$\phi_{ip}(\%) = \frac{\phi_{bulk} - \phi_p}{\phi_{bulk}} \quad (1)$$

Thus an understanding of the extent to which the packing and particle nature affects the measured bulk density can be extracted. Applying this approach to the three SDD materials above (Table 2), it can be demonstrated that there is significant variability in the distribution of porosity between intra and inter-particulate voids between the three samples

The results for the HPMC-AS SDD (Batch G) suggests that the packing within the powder bed is significantly more impactful in terms of the measured bulk density than the individual particle densities, whilst the morphological structure of the BMS-708163 (Batch F) material, with its large intra-particulate void spaces and relatively thin walled shell, is more likely to affect the measured bulk density.

This approach thus enables the separation of the particle density and the inter-particular packing elements of the measured

Table 2
True density and void space results.

Sample	Apparent true density (g/cm^3)	Void fraction (%)	
		Inter-particulate	Intra-particulate
BMS-817399, Batch E	1.187	59	41
BMS-708163, Batch F	1.314	42	58
HPMC-AS, Batch G	1.256	81	19

powder bulk density thereby making it possible to extract a true understanding of the measurement. More importantly, however, the measurements demonstrate that the bulk density measurement can be greatly affected by the morphological nature of the particles in addition to the powder bed packing.

Analysis of these hollow particles using this approach opens up new possibilities to accurately characterize and understand the powder properties of these classes of particles which cannot be done using the standard approaches utilised for solid particles.

5. Conclusions

A study was conducted to assess the applicability of X-ray microtomography to the characterisation of SDD particles. The results demonstrate that the approach can provide insight into the morphological characteristics of these hollow particles, and thereby a means to understand/predict the processability and performance characteristics of the bulk material. The application enables true 3-dimensional particle analysis with little or no sample preparation.

Due to the 3-dimensional volumetric nature of the application, the analysis was demonstrated to also be able to get a qualitative assess the impact of the drying rate on the morphological nature of the particles, thus providing further understanding with respect to particle morphology. Quantitative assessments of particle wall thickness, particle/void volume and thereby solid volume fraction can also be obtained providing further information which could be used to better characterize such particles.

Acknowledgements

The authors would like to thank Rao Mantri and Helen Hughes (Bristol-Myers Squibb) for support of the work, John Flynn, Luke Hunter and Rosy Manser (Carl Zeiss X-ray Microscopy) for enabling the XRM analysis and Bend Research (Bend, Oregon, USA) for manufacturing of the SDD materials used in this study.

References

Alonzo, D.E., Zhang, G.G.Z., Zhou, D., Gao, Y., Taylor, L.S., 2010. Understanding the behavior of amorphous pharmaceutical systems during dissolution. Pharm. Res. 27, 608–618.
Baird, J.A., Taylor, L.S., 2012. Evaluation of amorphous solid dispersion properties using thermal analysis techniques. Adv. Drug Deliv. Rev. 64, 396–421.
Berge, S.M., Bighley, L.D., Monkhouse, D.C., 1977. Pharmaceutical salts. J. Pharm. Sci. 66, 1–19.
Bhugra, C., Pikal, M.J., 2008. Role of thermodynamic, molecular, and kinetic factors in crystallization from the amorphous state. J. Pharm. Sci. 97, 1329–1349.
Chiou, W.L., Riegelman, S., 1971. Pharmaceutical applications of solid dispersion systems. J. Pharm. Sci. 60, 1281–1302.
Dobry, D.E., Settell, D.M., Baumann, J.M., Ray, R.J., Graham, L.J., Beyerinck, R.A., 2009. A model-based methodology for spray-drying process development. J. Pharm. Innov. 4, 133–142.
Elversson, J., Millqvist-Fureby, A., Alderborn, G., Elofsson, U., 2003. Droplet and particle size relationship and shell thickness of inhalable lactose particles during spray drying. J. Pharm. Sci. 92, 900–910.
Ford, J.L., 1986. The current status of solid dispersions. Pharm. Acta Helv. 61, 69–88.
Gamble, J.F., Ferreira, A.P., Tobyn, M., DiMemmo, L., Martin, K., Mathias, N., Schild, R., Vig, B., Baumann, J.M., Parks, S., Ashton, M., 2014. Application of imaging based tools for the characterisation of hollow spray dried amorphous dispersion particles. Int. J. Pharm. 465, 210–217.
Gillman, K.W., Starrett Jr, J.E., Parker, M.F., Xie, K., Bronson, J.J., Marcin, L.R., McElhone, K.E., Bergstrom, C.P., Mate, R.A., Williams, R., Meredith, J.E., Burton, C. R., Barten, D.M., Toyn, J.H., Roberts, S.B., Lentz, K.A., Houston, J.G., Zaczek, R., Albright, C.F., Decicco, C.P., MacOr, J.E., Olson, R.E., 2010. Discovery and evaluation of BMS-708163, a potent, selective and orally bioavailable γ-secretase inhibitor. ACS Med. Chem. Lett. 1, 120–124.
Graeser, K.A., Patterson, J.E., Zeitler, J.A., Gordon, K.C., Rades, T., 2009. Correlating thermodynamic and kinetic parameters with amorphous stability. Eur. J. Pharm. Sci. 37, 492–498.
Hancock, B.C., Parks, M., 2000. What is the true solubility advantage for amorphous pharmaceuticals? Pharm. Res. 17, 397–404.
Hancock, B.C., Shamblin, S.L., Zografi, G., 1995. Molecular mobility of amorphous pharmaceutical solids below their glass transition temperatures. Pharm. Res. 12, 799–806.
Hsieh, D.S., Yue, H., Nicholson, S.J., Roberts, D., Schild, R., Gamble, J.F., Lindrud, M., 2015. The secondary drying and the fate of organic solvents for spray dried dispersion drug product. Pharm. Res. 32, 1804–1816.
Leane, M.M., Sinclair, W., Qian, F., Haddadin, R., Brown, A., Tobyn, M., Dennis, A.B., 2013. Formulation and process design for a solid dosage form containing a spray-dried amorphous dispersion of ibipinabant. Pharm. Dev. Technol. 18, 359–366.
Leuner, C., Dressman, J., 2000. Improving drug solubility for oral delivery using solid dispersions. Eur. J. Pharm. Biopharm. 50, 47–60.
Maher, P.G., Auty, M.A.E., Roos, Y.H., Zychowski, L.M., Fenelon, M.A., 2015. Microstructure and lactose crystallization properties in spray dried nanoemulsions. Food Structure 3, 1–11.
Mayo, S.C., Miller, P.R., Wilkins, S.W., Davis, T.J., Gao, D., Gureyev, T.E., Paganin, D., Parry, D.J., Pogany, A., Stevenson, A.W., 2002. Quantitative X-ray projection microscopy: phase-contrast and multi-spectral imaging. J. Microsc. 207, 79–96.
Murtomaa, M., Savolainen, M., Christiansen, L., Rantanen, J., Laine, E., Yliruusi, J., 2004. Static electrification of powders during spray drying. J. Electrostat. 62, 63–72.
Patterson, A., Ferreira, A.P., Banks, E., Skeene, K., Clarke, G., Nicholson, S., Rawlinson-Malone, C., 2015. Modelling drug degradation in a spray dried polymer dispersion using a modified Arrhenius equation. Int. J. Pharm. 478, 348–360.
Paudel, A., Worku, Z.A., Meeus, J., Guns, S., Van Den Mooter, G., 2013. Manufacturing of solid dispersions of poorly water soluble drugs by spray drying: formulation and process considerations. Int. J. Pharm. 453, 253–284.
Rabinow, B.E., 2004. Nanosuspensions in drug delivery. Nat. Rev. Drug Discov. 3, 785–796.
Rautio, J., Kumpulainen, H., Heimbach, T., Oliyai, R., Oh, D., Järvinen, T., Savolainen, J., 2008. Prodrugs: design and clinical applications. Nat. Rev. Drug Discov. 7, 255–270.
Santella, J.B., Gardner, D.S., Duncia, J.V., Wu, H., Dhar, M., Cavallaro, C., Tebben, A.J., Carter, P.H., Barrish, J.C., Yarde, M., Briceno, S.W., Cvijic, M.E., Grafstrom, R.R., Liu, R., Patel, S.R., Watson, A.J., Yang, G., Rose, A.V., Vickery, R.D., Caceres-Cortes, J., Caporuscio, C., Camac, D.M., Khan, J.A., An, Y., Foster, W.R., Davies, P., Hynes, J., 2014. Discovery of the CCR1 antagonist, BMS-817399, for the treatment of rheumatoid arthritis. J. Med. Chem. 57, 7550–7564.
Serajuddln, A.T.M., 1999. Solid dispersion of poorly water-soluble drugs: early promises, subsequent problems, and recent breakthroughs. J. Pharm. Sci. 88, 1058–1066.
Tobyn, M., Brown, J., Dennis, A.B., Fakes, M., Gao, Q., Gamble, J., Khimyak, Y.Z., McGeorge, G., Patel, C., Sinclair, W., Timmins, P., Yin, S., 2009. Amorphous drug-PVP dispersions: application of theoretical, thermal and spectroscopic analytical techniques to the study of a molecule with intermolecular bonds in both the crystalline and pure amorphous state. J. Pharm. Sci. 98, 3456–3468.
Van den Mooter, G., Wuyts, M., Blaton, N., Busson, R., Grobet, P., Augustijns, P., Kinget, R., 2000. Physical stabilisation of amorphous ketoconazole in solid dispersions with polyvinylpyrrolidone K25. Eur. J. Pharm. Sci. 12, 261–269.
Vandecruys, R., Peeters, J., Verreck, G., Brewster, M.E., 2007. Use of a screening method to determine excipients which optimize the extent and stability of supersaturated drug solutions and application of this system to solid formulation design. Int. J. Pharm. 342, 168–175.
Vehring, R., Foss, W.R., Lechuga-Ballesteros, D., 2007. Particle formation in spray drying. J. Aerosol Sci. 38, 728–746.
Vehring, R., 2008. Pharmaceutical particle engineering via spray drying. Pharm. Res. 25, 999–1022.
Vicente, J., Pinto, J., Menezes, J., Gaspar, F., 2013. Fundamental analysis of particle formation in spray drying. Powder Technol. 247, 1–7.
Wegiel, L.A., Mauer, L.J., Edgar, K.J., Taylor, L.S., 2013. Crystallization of amorphous solid dispersions of resveratrol during preparation and storage-Impact of different polymers. J. Pharm. Sci. 102, 171–184.

Wong, J., D'sa, D., Foley, M., Chan, J., Chan, H.-K., 2014a. NanoXCT: a novel technique to probe the internal architecture of pharmaceutical particles. Pharm. Res. 31, 3085–3094.

Wong, J., Kwok, P.C.L., Noakes, T., Fathi, A., Dehghani, F., Chan, H.K., 2014b. Effect of crystallinity on electrostatic charging in dry powder inhaler formulations. Pharm. Res. 31, 1656–1664.

Yates, I., Regan, D., Ketner, R., Gamble, J.F., 2015. Calculation of Wall Thickness and Solid Volume Fraction of Spray Dried Particles by Mercury Intrusion. AAPS, Orlando, USA.

Yoshioka, M., Hancock, B.C., Zografi, G., 1995. Inhibition of indomethacin crystallization in poly(vinylpyrrolidone) coprecipitates. J. Pharm. Sci. 84, 983–986.